

# Supplementary Information for “Topological Phases in Graphene Nanoribbons: Junction States, Spin Centers and Quantum Spin Chains”

Ting Cao, Fangzhou Zhao, and Steven G. Louie\*

*Department of Physics, University of California at Berkeley, Berkeley, California 94720, USA and Materials Sciences Division, Lawrence Berkeley National Laboratory, 1 Cyclotron Road, Berkeley, California 94720, USA.*

\* [sglouie@berkeley.edu](mailto:sglouie@berkeley.edu)

## Section I: Calculation of the $Z_2$ invariant of AGNR within tight-binding model

We shall use the construction<sup>1</sup> that the  $Z_2$  invariant of a 1D system with inversion and/or mirror symmetries is given by  $(-1)^{Z_2} = \prod_n [p_n(\Gamma)p_n(X)]$ , where  $p_n(\Gamma)$  and  $p_n(X)$  are the parity eigenvalues of the state in the  $n$ th band at the  $\Gamma$  (center) and  $X$  (end) points of the 1D Brillouin zone, respectively. The product is over all occupied bands.

We start from the wavefunction of graphene to construct the wavefunctions of the armchair graphene nanoribbons (AGNRs) using proper boundary conditions, and then analyze the wavefunction parities of the AGNR. Considering only nearest neighbor hopping between the carbon  $\pi$  orbitals, the Hamiltonian of graphene is,

$$H^g(\mathbf{k}) = -t \begin{pmatrix} 0 & 1 + e^{ia\left(-\frac{\sqrt{3}}{2}k_x + \frac{1}{2}k_y\right)} + e^{ia\left(-\frac{\sqrt{3}}{2}k_x - \frac{1}{2}k_y\right)} \\ 1 + e^{ia\left(\frac{\sqrt{3}}{2}k_x + \frac{1}{2}k_y\right)} + e^{ia\left(\frac{\sqrt{3}}{2}k_x - \frac{1}{2}k_y\right)} & 0 \end{pmatrix}, \quad (1)$$

where  $t$  is the nearest neighbor hopping parameter,  $a$  the lattice constant,  $k_x$  and  $k_y$  the components of Bloch wavevector  $\mathbf{k}$  in the  $x$  and  $y$  directions, respectively (Fig. S1 and S2). The wavevector  $\mathbf{k}$  is measured from the center of the 2D Brillouin zone. The off-diagonal matrix element can be written as,

$$H_{12}^g(\mathbf{k}) = -t \left[ 1 + 2 \cos\left(\frac{ak_y}{2}\right) \cos\left(\frac{\sqrt{3}ak_x}{2}\right) + i \cdot (-2) \cos\left(\frac{ak_y}{2}\right) \sin\left(\frac{\sqrt{3}ak_x}{2}\right) \right]. \quad (2)$$

Using the pseudospin notation, the Hamiltonian of graphene can be rewritten as

$$H^g(\mathbf{k}) = -t \mathbf{h}(\mathbf{k}) \cdot \boldsymbol{\sigma}, \quad (3)$$

where  $\sigma_i$  are the Pauli matrices. The  $x$  and  $y$  components of the pseudo-magnetic field  $\mathbf{h}(\mathbf{k})$  are

$$h_x(\mathbf{k}) = 1 + 2 \cos\left(\frac{ak_y}{2}\right) \cos\left(\frac{\sqrt{3}ak_x}{2}\right), \quad (4)$$

and

$$h_y(\mathbf{k}) = 2 \cos\left(\frac{ak_y}{2}\right) \sin\left(\frac{\sqrt{3}ak_x}{2}\right). \quad (5)$$

By solving the Hamiltonian in Eq. 3, the energies  $E$  and eigenstates  $u^g$  of the conduction band and valence band from the carbon  $\pi$  orbitals at each  $\mathbf{k}$  point are

$$E_{\pm}(\mathbf{k}) = \pm t \sqrt{h_x^2(\mathbf{k}) + h_y^2(\mathbf{k})}, \quad (6)$$

$$u_{\pm}^g(\mathbf{k}) = \frac{1}{\sqrt{2}} \begin{pmatrix} e^{-i\phi(\mathbf{k})} \\ \mp 1 \end{pmatrix}, \quad (7)$$

where

$$e^{-i\phi(\mathbf{k})} = \frac{h_x(\mathbf{k}) - ih_y(\mathbf{k})}{\sqrt{h_x^2(\mathbf{k}) + h_y^2(\mathbf{k})}}. \quad (8)$$

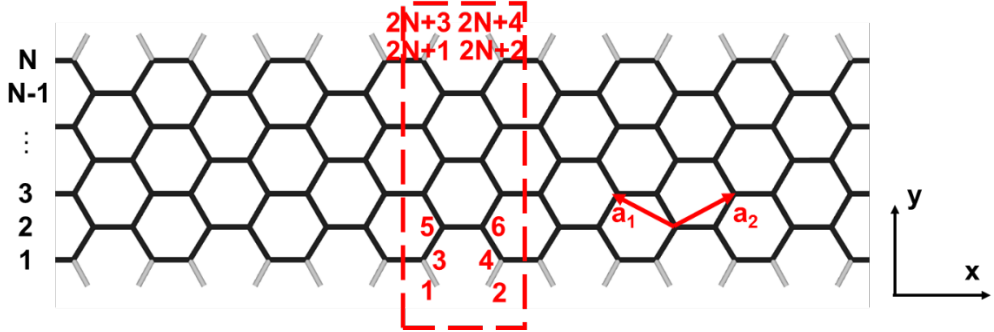


Fig. S1: Schematic structure of armchair graphene nanoribbons (AGNRs) with  $N$  rows of carbon atoms. The carbon-carbon bonds and carbon-hydrogen bonds are colored black and gray, respectively. The black numbers on the left label the row number of carbon atoms of the AGNR. The red numbers labels the carbon atom in a unit cell. The red dashed line denotes a unit cell of the AGNR. The red arrows are lattice vectors of graphene.

The “–“ and “+“ signs in the equations above denote the valence and conduction bands, respectively. To obtain the symmetry properties of wavefunctions, we now construct the wavefunctions of the AGNRs using the graphene wavefunctions with proper boundary conditions. With only nearest neighbor hopping between carbon atoms considered, the wavefunction of the AGNR must vanish beyond the carbon atoms at the armchair edge. Therefore, the boundary conditions for the AGNR with  $N$  rows of carbon atoms (see Fig. S1) are:

$$\langle 1|u_n(k_x)\rangle = \langle 2|u_n(k_x)\rangle = \langle 2N + 3|u_n(k_x)\rangle = \langle 2N + 4|u_n(k_x)\rangle = 0. \quad (9)$$

Here the orbitals “ $\langle 1|$ ”, “ $\langle 2|$ ”, “ $\langle 2N + 3|$ ”, and “ $\langle 2N + 4|$ ” are the  $\pi$  orbitals of the virtual carbon atoms located next to the outmost edge carbon atoms “3”, “4”, “ $2N + 1$ ”, and “ $2N + 2$ ”, respectively (Fig. S1).  $u_n(k_x)$  denotes the wavefunction of the  $n$ th band of an AGNR at the wavevector  $k_x$ .

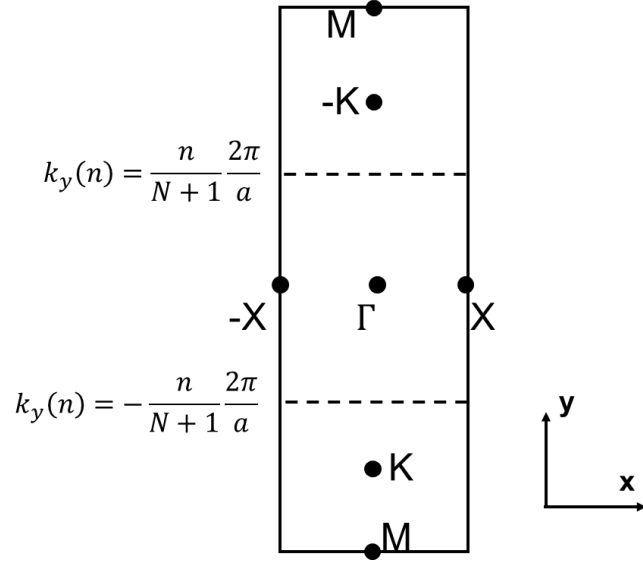


Fig. S2: Brillouin zone and high symmetry points of graphene. The dashed lines show the specific  $k$  path of which the wavefunctions of graphene constitute the  $n$ th band of an N-AGNR.

Using the boundary conditions in Eq. 9, we construct the wavefunctions of the occupied states in the  $n$ th band of the AGNR,

$$u_n(k_x) = \frac{1}{\sqrt{2}} [u^g(k_x, k_y(n)) - u^g(k_x, -k_y(n))]. \quad (10)$$

As shown in Fig. S2, the state in band  $n$  of wavevector  $k_x$  is composed of states of graphene with momentum  $(k_x, k_y)$  and  $(k_x, -k_y)$  with  $k_y$  given by the quantized value,

$$\frac{(N+1)a}{2} k_y(n) = n\pi, \quad (11)$$

or

$$k_y(n) = \frac{n}{N+1} \frac{2\pi}{a}, \quad (n = 1, 2, \dots, N). \quad (12)$$

The wavefunctions of the AGNR are then obtained from the wavefunctions of graphene. Using the unit cell of the AGNR shown in Fig. S1, the tight-binding wavefunction of the valence band of graphene is

$$u_{\pm}^g(k_x, k_y(n)) = \frac{1}{\sqrt{2N}} \begin{pmatrix} e^{i\mathbf{k}\cdot\mathbf{a}_1} \\ e^{-i\phi(\mathbf{k})} e^{i\mathbf{k}\cdot\mathbf{a}_2} \\ e^{-i\phi(\mathbf{k})} e^{ik_y a} \\ e^{ik_y a} \\ \dots \end{pmatrix}. \quad (13)$$

where the first component is the amplitude on site #3, the second component is the amplitude on site #4, etc. (Fig. S1) (Here for notational simplicity, we have just used “ $k_y$ ” for “ $k_y(n)$ ” on the right hand side of Eq. 13 and in subsequent equations below.) Using Eqs. 10 and 13, the explicit form of the  $n$ th valence band wavefunctions of the AGNR is

$$u_n(k_x, k_y(n)) = \frac{1}{\sqrt{N}} \begin{pmatrix} e^{-ik_x \frac{\sqrt{3}}{2} a} i \sin\left(k_y \frac{a}{2}\right) \\ e^{-i\phi(\mathbf{k})} e^{ik_x \frac{\sqrt{3}}{2} a} i \sin\left(k_y \frac{a}{2}\right) \\ e^{-i\phi(\mathbf{k})} i \sin(k_y a) \\ i \sin(k_y a) \\ \dots \end{pmatrix}. \quad (14)$$

We now analyze the wavefunction parities at the high symmetry points of the 1D Brillouin zone.

At the  $\Gamma$  point, the pseudo-magnetic field  $\mathbf{h}$  (Eqs. 4 and 5) in the graphene Hamiltonian is,

$$h_x(k_x = 0, k_y(n)) = 1 + 2 \cos\left(\frac{n\pi}{N+1}\right), \quad (15)$$

and

$$h_y(k_x = 0, k_y(n)) = 0. \quad (16)$$

We define a function  $f(\mathbf{k}) = e^{-i\phi(\mathbf{k})}$ . Using Eqs. 15 and 16, the value of  $f(\mathbf{k})$  for the band  $n$  at the  $\Gamma$  point is

$$f_n(\Gamma) = 1 \left( n < \frac{2(N+1)}{3} \right), \quad (17)$$

and

$$f_n(\Gamma) = -1 \left( n > \frac{2(N+1)}{3} \right). \quad (18)$$

Using Eqs. 6, 15, and 16, the energy of the band  $n$  at the  $\Gamma$  point is

$$E_n(\Gamma) = -t \left| 1 + 2 \cos\left(\frac{n\pi}{N+1}\right) \right|. \quad (19)$$

Using Eq. 14, we obtain the wavefunction of the band  $n$  at the  $\Gamma$  point,

$$u_n(\Gamma) = \frac{1}{\sqrt{N}} \begin{pmatrix} i \sin\left(\frac{n\pi}{N+1}\right) \\ f_n(\Gamma) i \sin\left(\frac{n\pi}{N+1}\right) \\ f_n(\Gamma) i \sin\left(\frac{2n\pi}{N+1}\right) \\ \dots \\ i \sin\left(\frac{2n\pi}{N+1}\right) \end{pmatrix}. \quad (20)$$

The wavefunction  $u_n(\Gamma)$  should be an eigenstate of the parity operator. The bulk unit cell shown in Fig. S1 contains both mirror (reflection) and inversion symmetry when  $N$  is even, and contains mirror symmetry when  $N$  is odd. In the following discussion, we use mirror as the parity operator. Under the mirror operator  $P$  which switches site #3 and #4, #5 and #6, etc.,  $u_n(\Gamma)$  transforms as

$$Pu_n(\Gamma) = f_n(\Gamma)u_n(\Gamma). \quad (21)$$

The wavefunction parity eigenvalue  $p$  of the state  $n$  at the  $\Gamma$  point is therefore

$$p_n(\Gamma) = f_n(\Gamma). \quad (22)$$

Taking all occupied states together, we have the product of their parity eigenvalues at the  $\Gamma$  point as

$$\Pi_n p_n(\Gamma) = \Pi_n f_n(\Gamma). \quad (23)$$

For  $N = 3m$  and  $3m + 1$  ( $m$  is a positive integer),

$$\Pi_n p_n(\Gamma) = (-1)^m. \quad (24)$$

For  $N = 3m + 2$ . The system does not have a gap in this simple tight-binding model, as one of the bands passes through the K point of graphene. However, a sizeable band gap does exist in

these graphene nanoribbons from *ab initio* density functional theory (DFT) calculations<sup>2</sup>. The presence of the band gap in most part is due to the contraction of carbon-carbon bond on the armchair edges, leading to a stronger electron hopping between these edge carbon atoms. Using bigger hopping parameters on the edge carbon atoms, the tight-binding band gap approaches the *ab initio* results. We thus calculate the  $\Gamma$  point wavefunctions in these cases ( $N = 3m + 2$ ) using this method, and find that the relation  $\Pi_n p_n(\Gamma) = (-1)^m$  still holds.

At the X point, the pseudo-magnetic field in Eqs. 4 and 5 is

$$h_x \left( k_x = \frac{\pi}{\sqrt{3}a} \right) = 1, \quad (25)$$

and

$$h_y \left( k_x = \frac{\pi}{\sqrt{3}a} \right) = 2 \cos \left( \frac{n\pi}{N+1} \right). \quad (26)$$

The  $f$  function for the state in the band  $n$  at the X point is (using Eq. 8)

$$f_n(X) = \frac{1 - 2i \cos \left( \frac{n\pi}{N+1} \right)}{\sqrt{1 + 4 \cos^2 \left( \frac{n\pi}{N+1} \right)}}. \quad (27)$$

The energy of the state in band  $n$  at the X point is

$$E_n(X) = -t \sqrt{1 + 4 \cos^2 \left( \frac{n\pi}{N+1} \right)}. \quad (28)$$

The wavefunction of the state in band  $n$  at the X point is

$$u_n(X) = \frac{1}{\sqrt{N}} \begin{pmatrix} \sin \left( \frac{n\pi}{N+1} \right) \\ -f_n(X) \sin \left( \frac{n\pi}{N+1} \right) \\ f_n(X)i \sin \left( \frac{2n\pi}{N+1} \right) \\ i \sin \left( \frac{2n\pi}{N+1} \right) \\ \dots \end{pmatrix}. \quad (29)$$

$u_n(X)$  in this form is not an eigenstate of the parity operator. However, band  $N + 1 - n$  is degenerate with the band  $n$  at the X point. These two bands are doubly degenerate owing to the

mirror symmetry of the system. This can be verified using our tight-binding model, which gives the energy of the band  $N + 1 - n$  at the X point to be

$$E_{N+1-n}(X) = -t \sqrt{1 + 4 \cos^2 \left( \frac{n\pi}{N+1} \right)} = E_n(X). \quad (30)$$

The wavefunction of the state in band  $N + 1 - n$  at the X point is

$$u_{N+1-n}(X) = \frac{1}{\sqrt{N}} \begin{pmatrix} \sin \left( \frac{n\pi}{N+1} \right) \\ -f_{N+1-n}(X) \sin \left( \frac{n\pi}{N+1} \right) \\ -f_{N+1-n}(X)i \sin \left( \frac{2n\pi}{N+1} \right) \\ -i \sin \left( \frac{2n\pi}{N+1} \right) \\ \dots \end{pmatrix}, \quad (31)$$

where

$$f_{N+1-n}(X) = \frac{1 + 2i \cos \left( \frac{n\pi}{N+1} \right)}{\sqrt{1 + 4 \cos^2 \left( \frac{n\pi}{N+1} \right)}} = f_n^*(X). \quad (32)$$

The degenerate states with wavefunctions  $u_n(X)$  and  $u_{N+1-n}(X)$  are orthogonal to each other, and they could form two states with opposite parity through a unitary transformation. They together give rise to

$$p_n(X)p_{N+1-n}(X) = -1. \quad (33)$$

When  $N$  is odd, the only singly degenerate band is  $n = \frac{N+1}{2}$  with wavefunction

$$u_{\frac{N+1}{2}}(X) = \frac{1}{\sqrt{N}} \begin{pmatrix} 1 \\ -1 \\ 0 \\ 0 \\ \dots \end{pmatrix}. \quad (34)$$

So we obtain the parity of this state  $u_{\frac{N+1}{2}}(X)$  being

$$p_{\frac{N+1}{2}}(X) = -1. \quad (35)$$

When  $N$  is even, all bands are doubly degenerate at  $X$ .

We now look at all occupied bands at  $X$  using Eqs. 33 and 35:

For  $N = 4r$  and  $4r + 3$  ( $r$  is a positive integer),

$$\Pi_n p_n(X) = 1. \quad (36)$$

For  $N = 4r + 1$  and  $4r + 2$ ,

$$\Pi_n p_n(X) = -1. \quad (37)$$

Now we have the products of the parity eigenvalues of states at  $\Gamma$  and  $X$ ,

$$\Pi_n p_n(\Gamma) p_n(X) = (-1)^{\lfloor \frac{N}{3} \rfloor} (-1)^{\lfloor \frac{N+1}{2} \rfloor}. \quad (38)$$

Therefore, we obtain the value of  $Z_2$  of AGNR with zigzag' ( $N = \text{odd}$ ) and zigzag ( $N = \text{even}$ ) terminations given in Eqs. 4 and 5 in the main text.

We have also derived the value of  $Z_2$  for the bearded ( $N = \text{even}$ ) and zigzag ( $N = \text{odd}$ ) terminations that have inversion symmetry using similar methods. The products of the parity eigenvalues of states at  $\Gamma$  and  $X$  are  $(-1)^{\lfloor \frac{N}{3} \rfloor}$  and  $-(-1)^{\lfloor \frac{N}{3} \rfloor} (-1)^{\lfloor \frac{N+1}{2} \rfloor}$  for the bearded ( $N = \text{even}$ ) and zigzag ( $N = \text{odd}$ ) terminations, respectively. These results together give the formulae presented in Eqs. 3-6 in the main text.

Instead of Table I in the main text, we display our main results in a slightly different form in Fig. S3, which directly gives the numerical values of  $Z_2$  for the different AGNRs using the formulae derived above and listed in Table 1 in the main text.

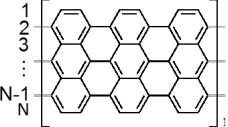
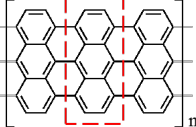
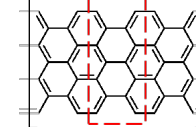
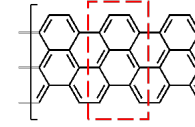
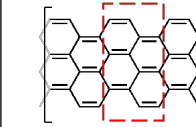
	N = Odd				N = Even			
Termination type	Zigzag	Zigzag'	Zigzag	Bearded				
Unit cell shape								
Bulk Symmetry	Inversion/mirror		Inversion/mirror		Mirror		Inversion	
N mod 12	1, 3, 11	5, 7, 9	1, 3, 11	5, 7, 9	0, 8, 10	2, 4, 6	4, 10	0, 2, 6, 8
$Z_2$	0	1	1	0	0	1	1	0

Fig. S3: Categorization of topology of armchair graphene nanoribbons (AGNRs). The nanoribbons are identified according to the different ribbon width  $N$  (given by the number of rows of carbon atoms shown in the first row of the figure) and the type of termination (labelled in the second row). Schematics of the structure is plotted in the third row. The bulk unit cell of each structure that is commensurate with the termination is indicated by the dashed red rectangle. The bulk symmetry, the value  $N \bmod 12$ , and the  $Z_2$  number calculated using our explicit  $Z_2$  formulae are shown in the fourth, fifth, and sixth row, respectively.

Our results shown in Table 1 of the main text and in Fig. S3 have been verified by explicit density functional theory (DFT) calculations on selected cases. We have also used a supercell approach to calculate the electronic structure of finite length AGNRs in vacuum that have different types of terminations, and count the number of end states in the bandgap localized at the termination. The number of end states (without counting the spin degree of freedom) at the termination is dictated by the value of  $Z_2$  of the corresponding structure in Fig. S3: even and odd number of end states appear for  $Z_2 = 0$  and  $Z_2 = 1$ , respectively. Also, for a given type of termination, the number of localized end states would in general increase with ribbon width  $N$ .

## Section II: 9AGNR/5AGNR junctions.

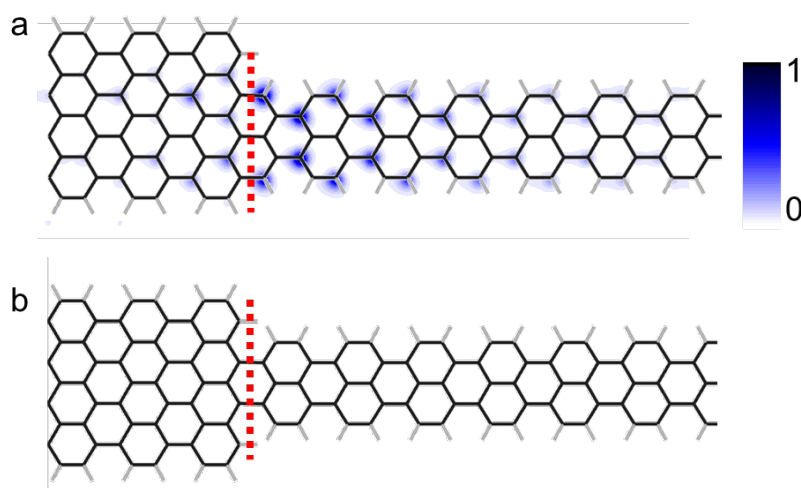


Fig. S4. Heterojunctions formed with  $N=9$  and  $N=5$  armchair graphene nanoribbons (9AGNR/5AGNR) between two (a) topologically inequivalent segments and (b) topologically equivalent segments. The red dashed line denotes the interface between the two nanoribbons. The carbon-carbon and carbon-hydrogen bonds are colored black and gray, respectively. The color scale shows the charge density of the localized midgap junction state. The charge density is integrated along the out-of-plane direction, and normalized to the largest value.

## Section III: Boron doped GNRs

The wavefunctions plotted in Fig. 2c in the main text come from the defect-state orbitals (not orbitals of a boron dimer in vacuum) associated with a boron pair in 7AGNR in the supercell shown in Fig. S5, which is well-separated from a nearby pair in the next supercell, corresponding to the dilute doping limit.

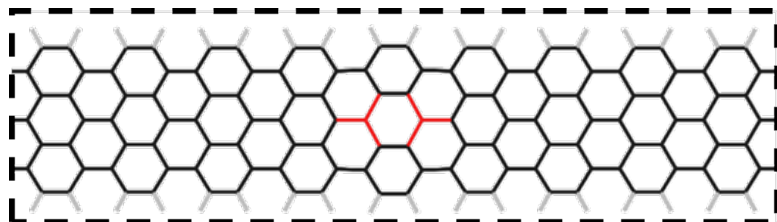


Fig. S5: Supercell of a boron dimer doped graphene nanoribbon at dilute dopant concentrations. The carbon-carbon, carbon-boron, and carbon-hydrogen bonds are colored black, red and gray, respectively.

In the dilute doping limit, two defect or dopant states (with no  $k$ -dependent) exist in the band gap of the 7AGNR. The energy of these two dopant states in this limit are nearly degenerate, with a separation of  $< 20$  meV. The lower energy state is occupied, and the higher energy state is unoccupied for the charge neutral system at zero temperature. As the dopant concentration increases, the two dopant states interact with those from the neighboring supercells and develop, in a highly unusual way, into two non-intersecting dopant bands. These two dopant bands are very flat owing to quantum level repulsion. The gap between these two flat dopant bands increases as the distance between adjacent boron pairs decreases (i.e., the concentration increases).

To explicitly show how the wavefunction character of each of the dopant bands changes from the BZ center to the BZ boundary, we calculate the charge density of the dopant-band states at the two high symmetry points of the 1D Brillouin zone, at 1 Å above the nanoribbon plane (Fig. S6). For the upper dopant band, from the BZ center to the BZ boundary, the wavefunction character changes from the s-like defect orbital (Fig. S6 b) to the p-like defect orbital (Fig. S6 c). For the lower dopant band, from the BZ center to the BZ boundary, the wavefunction character changes from the p-like orbital (Fig. S6 d) to the s-like defect orbital (Fig. S6 e).

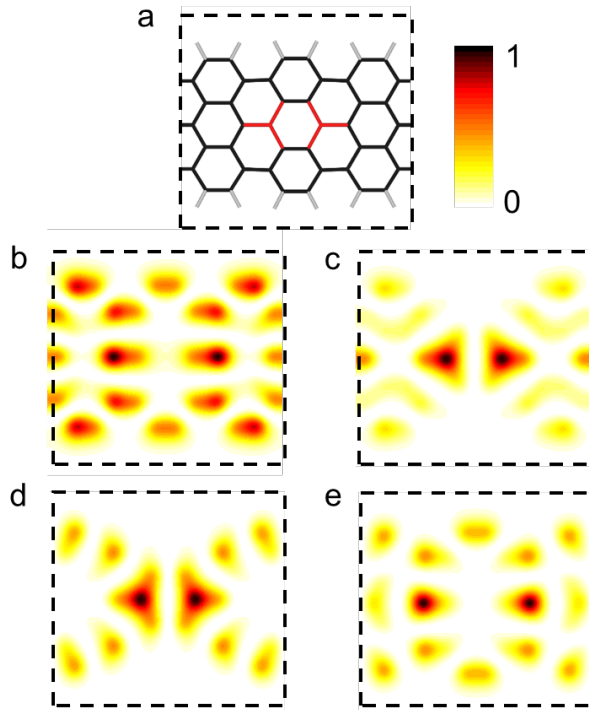


Fig. S6: Charge density of the dopant-band states at the high symmetry points of the 1D Brillouin zone (BZ). (a) Structure of an N=7 armchair graphene nanoribbon periodically doped with boron pairs (B2-7AGNR). The carbon-carbon, carbon-boron, and carbon-hydrogen bonds are colored black, red and gray, respectively. The dashed black rectangle indicates the unit cell of the system studied. (b-e) Charge density of the upper dopant band states at BZ center (b) and BZ edge (c), and of the lower dopant band states at BZ center (d) and BZ edge (e), plotted at 1 Å above the nanoribbon plane. The charge density is normalized to its maximum value in each plot.

#### Section IV: Robustness of topological nontrivial AGNR end states against local perturbations

Regarding to the robustness of GNR end states, we would like to point out that the topological phases of the GNR systems are protected by spatial symmetries, such as mirror reflection and spatial inversion. Breaking these spatial symmetries at the terminating unit cell could in principle change the end states. However, for small width GNR systems, the band gaps are in the order of a few eVs, which are orders of magnitude larger than those of usual 2D/3D topological insulators, e.g.  $\text{Bi}_2\text{Se}_3$ . The presence of mid-gap end states is therefore quite robust against local perturbations. For example, at the end of an N=7 AGNR

with zigzag termination, local perturbations to the end carbon atoms with integrated strength  $W$  of  $0 < W < 4$  eV are unable to destroy the end states (discussed below).

To examine the robustness of vacuum end states in GNRs against local perturbations, we take a finite length (3.5 nm)  $N=7$  AGNR with zigzag termination on both ends as a typical system, and perform tight-binding calculations on its electronic structure with an applied perturbation of varying strength and configuration to the atoms at one end. As we have discussed in the main text,  $N=7$  AGNR with zigzag termination has  $Z_2 = 1$ , and therefore has 1 end state localized at each end. In our tight-binding calculations of the pristine structure, we include only nearest-neighbor hopping between the carbon  $\pi$  orbitals. The hopping parameter  $t$  is set to -2.7 eV, and the carbon onsite energy is set to zero.

For the perturbed system, we first change separately the onsite energy of the carbon  $\pi$  orbital on the different atoms of the zigzag termination (labeled by 1 – 4 in Fig. S7 below) to mimic the effects of local electrostatic potential variations. For each orbital, we change its onsite energy from 0 eV to 4 eV, and find that the number of end states remains unchanged.

We also change the hopping matrix element between two adjacent carbon  $\pi$  orbitals at the zigzag termination to mimic the effect of lattice distortion. In each case, the hopping matrix element between neighboring carbon  $\pi$  orbitals (labeled by a – e in Fig. S7) is tuned from -6.7 eV to 1.3 eV. We find that the number of end states again remains unchanged in all these cases.

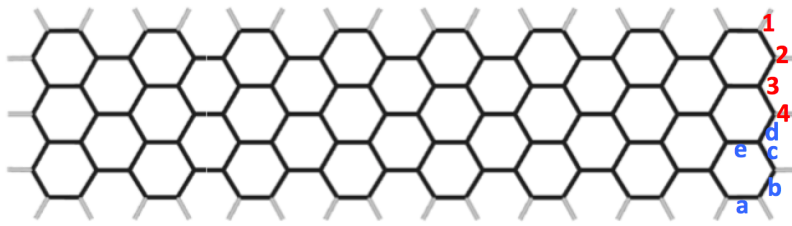


Fig. S7. Structure of a finite length 7AGNR in vacuum used in the tight-binding calculations to test the robustness of end states. We change separately the onsite energy of the 4 atoms labeled by 1 – 4. We also change the hopping matrix elements, labeled by a – e, between carbon  $\pi$  orbitals.

## **References:**

1. Fu, L. & Kane, C. L. Topological insulators with inversion symmetry. *Phys. Rev. B* **76**, 045302 (2007).
2. Son, Y.-W., Cohen, M. L. & Louie, S. G. Energy gaps in graphene nanoribbons. *Phys. Rev. Lett.* **97**, 216803 (2006).